

## THE SDSS–HET SURVEY OF *KEPLER* ECLIPSING BINARIES: SPECTROSCOPIC DYNAMICAL MASSES OF THE *KEPLER*-16 CIRCUMBINARY PLANET HOSTS<sup>1</sup>

CHAD F. BENDER, SUVRATH MAHADEVAN, ROHIT DESHPANDE, JASON T. WRIGHT, ARPITA ROY, RYAN C. TERRIEN, STEINN SIGURDSSON, LAWRENCE W. RAMSEY, DONALD P. SCHNEIDER, AND SCOTT W. FLEMING

Department of Astronomy & Astrophysics, Pennsylvania State University, 525 Davey Lab, University Park, PA-16802  
Center for Exoplanets & Habitable Worlds, Pennsylvania State University

### ABSTRACT

We have used high-resolution spectroscopy to observe the *Kepler*-16 eclipsing binary as a double-lined system, and measure precise radial velocities for both stellar components. These velocities yield a dynamical mass-ratio of  $q = 0.2994 \pm 0.0031$ . When combined with the inclination,  $i = 90^\circ 3401_{-0.0019}^{+0.0016}$ , measured from the *Kepler* photometric data by Doyle et al. (2011), we derive dynamical masses for the *Kepler*-16 components of  $M_A = 0.654 \pm 0.017 M_\odot$  and  $M_B = 0.1959 \pm 0.0031 M_\odot$ , a precision of 2.5% and 1.5% respectively. Our results confirm at the  $\sim 2\%$  level the mass-ratio derived by D11 with their photometric-dynamical model,  $q = 0.2937 \pm 0.0006$ . These are among the most precise spectroscopic dynamical masses ever measured for low-mass stars, and provide an important direct test of the results from the photometric-dynamical modeling technique.

*Subject headings:* binaries: eclipsing — binaries: spectroscopic — stars: fundamental parameters — stars: individual (*Kepler*-16) — stars: low-mass — techniques: radial velocities

### 1. INTRODUCTION

The NASA *Kepler* space mission is monitoring about 150,000 stars with a photometric precision of a few parts per million in an effort to find transiting Earth mass planets (Borucki et al. 2010). This program has led to the discovery of more than 2000 eclipsing binaries (EBs) in the *Kepler* field, for which public light-curves now exist (Prša et al. 2011; Slawson et al. 2011). These light-curves constrain the inclination angle,  $i$ , of the orbit, and when coupled with radial velocities (RVs) derived from double-lined spectroscopic observations (SB2), they yield precise dynamical masses. Detailed modeling of the light-curves also provides radii measurements for many of these targets. Here, we investigate the properties of the EB *Kepler*-16A & B (Doyle et al. 2011, hereafter, D11), which hosts a circumbinary planet *Kepler*-16b. D11 used a photometric-dynamical model (hereafter, PDM) to solve the *Kepler* light-curve data for the Newtonian motion of the three body system, and derived precise masses ( $\lesssim 0.5\%$  for the stars, and  $\lesssim 5\%$  for the planet) and radii ( $\sim 0.3\%$  for all bodies). Our objective here is to use the traditional RV based approach to independently measure the masses for *Kepler*-16A & B.

Fundamental measurements of a diverse sample of stars are critical for testing theoretical stellar mass-radius relationships, but placing meaningful constraints on models requires measurement precision of better than 2-3% (Torres et al. 2010). The DEBCat<sup>2</sup> catalog lists the physical properties of detached EBs with mass and radius known to better than  $\sim 2\%$ , following the criteria of Andersen (1991), and currently includes about

130 such systems. Most DEBCat stars are solar mass or greater, and models and observations agree in this regime. Constraints on the low-mass population are much sparser: DEBCat includes only 28 stars with  $M < 0.8 M_\odot$ , and only 3 with  $M < 0.3 M_\odot$ . Many of these have radii 10-20% larger than predicted by models (e.g., López-Morales 2007; López-Morales & Shaw 2007; Torres et al. 2010). Current theories propose that increased magnetic fields due to tidal locking produce starspots, resulting in decreased effective temperature. In addition, the magnetic fields can suppress convection in the outer atmosphere of the star. Both processes can yield inflated stellar radii relative to current models (Ribas 2006; Chabrier et al. 2007).

Adequately testing these theories requires expanding the sample of low-mass stars with precisely measured masses and radii, and spectroscopic observations of the *Kepler* EBs as SB2s can yield such a sample. Because the *Kepler* EBs have a wide range of orbital periods,  $P$ , and are relatively faint, a comprehensive RV survey is impractical. Various groups are focusing on sub-samples, such as transiting hot compact objects (Coughlin et al. 2011) or low-mass stars (Rowe et al. 2010). We are targeting  $\sim 100$  *Kepler* EBs with light curves that predict low-mass secondaries. Our objective is to measure the dynamical masses of these stars to 3% or better. Binaries with mass ratio,  $q = M_2/M_1$ , much less than one, have a secondary-to-primary flux ratio,  $\alpha$ , that is very small in visible light, but more favorable in the infrared. Such systems can often be efficiently solved as SB2s by combining visible light spectroscopy that precisely measures the primary RVs, with a smaller number of infrared observations that detect the secondary (e.g., Bender & Simon 2008).

We are observing our EBs with the H-band APOGEE spectrograph (Wilson et al. 2010), which is part of the Sloan Digital Sky Survey-III (Eisenstein et al. 2011). APOGEE's multi-object capabilities can survey a large

cbender@psu.edu

<sup>1</sup> Based on observations obtained with the Hobby-Eberly Telescope, which is a joint project of the University of Texas at Austin, the Pennsylvania State University, Stanford University, Ludwig-Maximilians-Universität München, and Georg-August-Universität Göttingen.

<sup>2</sup> <http://www.astro.keele.ac.uk/jkt/debcats/>

number of EBs as SB2s, but provide a small number of epochs for each (typically from three to six). We are supplementing these observations with visible light spectroscopy from the fiber-fed High Resolution Spectrograph (hereafter, HRS; Tull 1998) on the 9.2m Hobby-Eberly Telescope (hereafter, HET; Ramsey et al. 1998). The HET queue-scheduled operation (Shetrone et al. 2007), combined with the precise  $P$  measured by *Kepler*, provides efficient observations of our EB sample at targeted orbital phases. In most cases our HRS spectra provide single-lined binary orbits (SB1s), but some, including the results presented here, have the sensitivity to directly solve an EB as an SB2.

Here, we present new observations of the circumbinary planet system Kepler-16 as an SB2. Section 2 describes the Kepler-16 system and discusses the importance of circumbinary planet systems. Sections 3, 4, and 5, present our observations, data analysis, and orbit fitting procedures. Section 6 compares our results with D11 and draws some relevant conclusions. Future papers will describe our ongoing survey in more detail and present dynamical results from additional EBs.

## 2. CIRCUMBINARY PLANETS & THE KEPLER-16 SYSTEM

Planets orbiting binary stars, or circumbinary planets, likely provide key insights towards understanding planet formation processes, so discovering and characterizing these systems is a high priority. However, such planets are not well suited to discovery with precision RV techniques that have yielded most of the confirmed planet population because measuring precise velocities in a binary spectrum is challenging. Attempts to circumvent this problem by combining RVs with interferometric observations have resulted in some of the most precise stellar masses known, but have not yet detected planets (Konacki 2005b; Konacki et al. 2010). Measuring transit timing variations of EBs has become the technique of choice in circumbinary planet searches. Eclipse timing variation signals, interpreted as due to a planetary mass object, have been detected around HW Virginis, CM Dra, SS Serpens, and HU Aq, although the planetary interpretation has also been questioned (e.g., Horner et al. 2011; Wittenmyer et al. 2012).

Three circumbinary planets have recently been identified with *Kepler* photometry, and characterized through the application of a three-body PDM (Carter et al. 2011): Kepler-16b (D11), Kepler-34b, and Kepler-35b (Welsh et al. 2012). The Kepler-16 system is particularly interesting for constraining stellar mass-radius relationships because its stellar components are both low-mass. From the PDM, D11 determined that Kepler-16 has  $q = 0.2937 \pm 0.0006$  (J. Carter, private communication). When combined with single-lined TRES spectroscopy, they derived masses of  $M_A = 0.6897 \pm 0.0035$  and  $M_B = 0.20255 \pm 0.00065$ , for Kepler 16-A & B respectively. Their spectroscopy was unable to detect Kepler-16B, which has  $\alpha = 0.015$  in the *Kepler* bandpass.

Given the small, but significant, discrepancies between stellar radii measured for low-mass stars and current stellar models, obtaining robust absolute mass measurements for individual systems is critical to anchor the absolute offset for the models. The PDM provides an estimate of stellar masses based on a three-body Newtonian model, and is a relatively new and powerful technique

that may be applicable to numerous systems with precise photometry and multiple transiting objects. An important part of scientific investigation is the independent confirmation of results and techniques, preferably using different instruments and measurements of independent variables. Observations of a binary as an SB2 use a Keplerian model (hereafter, KM) to estimate  $q$  and absolute masses, and are a well established technique. The SB2 observations of Kepler-16 we present here directly test the PDM results.

## 3. OBSERVATIONS WITH THE HOBBY-EBERLY TELESCOPE

We obtained six observations of Kepler-16 with the HRS, from September through October 2011, using the 316g7940 cross-disperser, a 2" diameter fiber that encompassed both stars, and a slit providing  $R \sim 30,000$ . Each observation was a 1200 s integration, which yielded  $S/N \sim 300$  per resolution element, and was bracketed before and after with a ThAr hollow-cathode lamp exposure for wavelength calibration. We used the same procedure on two known single stars, HD17230 and GJ905, to serve as spectral templates for Kepler-16A & B, respectively. HD17230 has spectral type K6V, with  $T_{\text{eff}} = 4442 \pm 44\text{K}$ ,  $\log g = 4.89 \pm 0.06$ , and  $[M/H] = 0.02 \pm 0.03$  (Valenti & Fisher 2005). GJ905 has spectral type M5.5V, with  $T_{\text{eff}} = 2800 \pm 100\text{K}$ , and  $[M/H] = 0.00 \pm 0.25$  (Leggett et al. 2000).

We extract HRS spectra using a custom optimal extraction pipeline, similar to that described by Cushing et al. (2004), written by us in the Interactive Data Language (IDL). This pipeline automatically performs basic image processing, including overscan correction, bias subtraction, and flat fielding. It then automatically traces the spectral orders in each HRS target observation, computes the optimal fiber profile for each order, and carries out the extraction. ThAr calibration spectra are extracted in a similar manner, using a fiber profile determined from exposures of twilight sky or a flat lamp observed through the target fiber. A multi-order solution equating pixel position to wavelength is fit to the ThAr spectrum using the linelist of Murphy et al. (2007), and then applied to the corresponding target spectrum. We found no significant difference between the two ThAr frames that bracketed each observation, indicating that HRS was stable throughout each integration, and so arbitrarily used the later ThAr solution for each observation. To facilitate use by other investigators, we have placed our extracted Kepler-16 spectra in the NASA Exoplanet Archive<sup>3</sup>.

We used a synthetic telluric absorption function generated with the LBLRTM atmospheric model (Clough et al. 2005) to identify spectral regions contaminated by telluric absorption, and excluded them from subsequent analyzes. We removed sharp night-sky OH emission features by linearly interpolating over them. In the 316g7940 configuration many orders overlap off-blaze wavelengths. We combined these orders into five contiguous segments which were free of telluric absorption: 6180–6270Å, 6340–6450Å, 6600–6850Å, 7440–7580Å, and 8460–8870Å. In each bandpass the Kepler-16 binary has a different  $\alpha$ . Using BT-Settl models (Allard et al. 2011)

<sup>3</sup> <http://exoplanetarchive.ipac.caltech.edu>

**Table 1**  
HRS Radial Velocity Measurements of Kepler-16A & B

UT Date	BJD - 2,400,000	Orbital Phase	$V_A$ (km s $^{-1}$ )	$V_B$ (km s $^{-1}$ )
2011 Sep 27	55831.677860	0.607	$-39.175 \pm 0.026$	$-15.39 \pm 0.80$
2011 Oct 6	55840.643682	0.825	$-47.615 \pm 0.025$	$13.32 \pm 1.03$
2011 Oct 8	55842.631447	0.874	$-46.510 \pm 0.030$	$8.88 \pm 1.08$
2011 Oct 15	55849.627832	0.044	$-30.288 \pm 0.023$	$-44.34 \pm 0.63$
2011 Oct 20	55854.601732	0.165	$-21.244 \pm 0.026$	$-75.20 \pm 0.82$
2011 Oct 24	55858.588560	0.262	$-20.917 \pm 0.025$	$-76.80 \pm 0.78$

that correspond to the  $T_{\text{eff}}$ ,  $\log(g)$ , and  $[\text{Fe}/\text{H}]$  derived by Winn et al. (2011) and D11 (and shown in Fig 1) we estimate the  $\alpha$  in each bandpass to be 0.00522, 0.00743, 0.00780, 0.0228, and 0.0286, respectively.

#### 4. SB2 ANALYSIS

The cross-correlation algorithm TODCOR (Zucker & Mazeh 1994) simultaneously cross-correlates two template spectra against a target spectrum containing the blended light from a binary to disentangle the component RVs. We used TODCOR, along with the HD17230 and GJ905 templates, to measure the RVs of Kepler-16A & B in our HRS spectra. Following Zucker et al. (2003), we solved each bandpass independently with  $\alpha$  locked to the corresponding value estimated in §3, and combined the resulting correlation surfaces with a maximum-likelihood analysis (Zucker 2003). TODCOR is more sensitive to the RV of each component than to the  $\alpha$ , and in high-contrast binaries where the flux from the primary dominates, a discrepancy of a factor of 2–3 between the chosen  $\alpha$  and the true value can still yield equivalent RVs. Similarly, small mismatches in the target and template metallicity primarily affect the ability of TODCOR to derive an optimal  $\alpha$ , and do not affect the measured RVs (Bender et al. 2005). By locking  $\alpha$  across all HRS epochs, we minimize the effect on the RVs of discrepancies with the BT Settl  $\alpha$  or template metallicity mismatch.

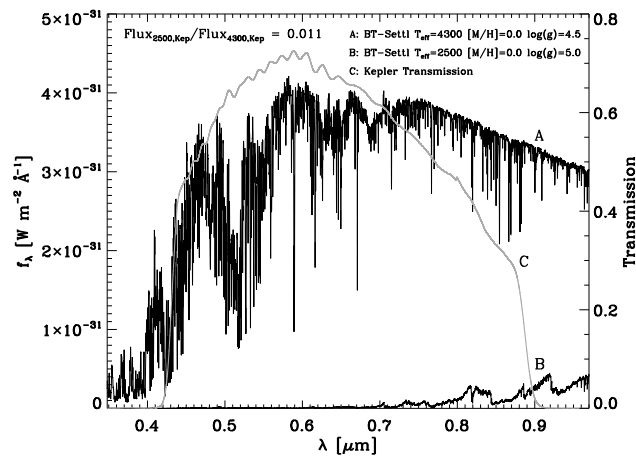


**Figure 1.** BT-Settl models corresponding to Kepler-16A & B, plotted along with the *Kepler* response function. The  $\alpha$  of these models in the *Kepler* bandpass,  $\sim 1\%$ , is consistent with the value measured by D11; in the HRS bandpasses  $\alpha$  ranges from  $\sim 0.5\%$  to  $\sim 3\%$ .

In analyzing each observation we restricted the secondary velocity search to the range bounded by  $q = 1$  and the minimum-mass from the mass-function, which are constrained by the SB1 solution and the orbital phase, and chose the largest amplitude peak in this range. The component RVs,  $V_A$  and  $V_B$ , are measured by fitting the top six to eight points of this peak with a quadratic. Uncertainties are derived from the maximum-likelihood formalism of Zucker (2003), which accounts for spectral bandwidth, correlation peak sharpness, and the spectral line S/N, but may exclude systematic uncertainties due to the instrument or templates. Our templates share many of the same spectral features, so the M6V template correlates reasonably well with the Kepler-16A spectrum and results in a spurious peak in secondary velocity equal to  $V_A$ . In all observations except for 2011 Oct 15, the true secondary peak was well separated from the spurious peak and could be measured directly. For 2011 Oct 15, the secondary peak was blended in the blue wing of the spurious peak. We fit the unblended portion of the spurious peak with a Gaussian and subtracted it, which provided a clean secondary peak to measure  $V_B$ .

Table 1 lists the midpoint Barycentric Julian Date (BJD), the corresponding orbital phase, and our measured RVs for each HRS observation. Figure 2 shows cuts through the correlation surfaces, along with the measured RVs. We are monitoring the HRS long-term stability by observing stars known to be intrinsically stable to a few  $\text{ms}^{-1}$ . These observations, taken over many months, show RV variations with  $\text{RMS} \sim 20 \text{ ms}^{-1}$ , which is less than the  $V_A$  uncertainties reported in Table 1. The secondary peaks for 2011 Oct 06 and 2011 Oct 08 are weaker than for the other dates (Figure 2); this is likely due to lower intrinsic S/N, and is reflected in the uncertainties reported in Table 1.

#### 5. DERIVATION OF ORBITAL PARAMETERS AND DYNAMICAL STELLAR MASSES

Measuring Kepler-16 as an SB2 allows us to use a KM to derive a dynamical mass-ratio,  $q$ , and dynamical masses,  $M_A$  and  $M_B$ , for the stellar binary. These values constrain the stellar mass-radius relationship and test the 23 parameter PDM used by D11. For reference, Table 2 lists the relevant orbital parameters from D11. For our purposes,  $q$  is the most fundamental parameter describing the EB, and can be derived without any orbit modeling using the procedure of Wilson (1941). The “Wilson Test” fits a straight line through a plot of  $V_A$  versus  $V_B$ : the negative slope of this line directly yields  $q = 0.2986 \pm 0.0031$ .

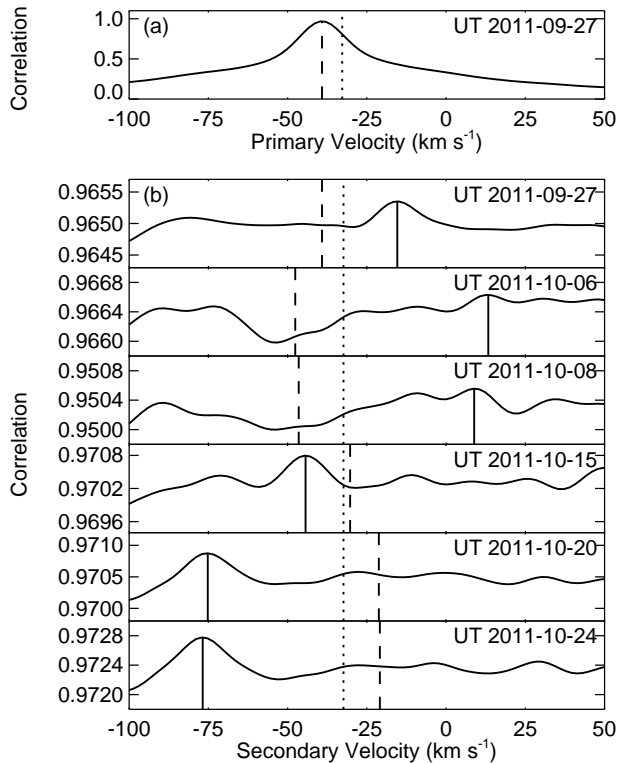


**Figure 2.** Cuts through correlation surfaces vs. velocity, showing (a) an example primary peak, and (b) secondary peaks for each observation. Primary cuts not shown have the same general shape as (a). Vertical dashed and solid lines indicate the measured  $V_A$  and  $V_B$ , respectively. Dotted lines show the systemic velocity,  $\gamma_A$ . The spurious secondary peak at  $V_A=V_B$  (§4) has been removed for clarity.

The *Kepler* photometry timing constrains the orbital period,  $P$ , and the time of transit,  $T_t$ , with precision that cannot be improved by new spectroscopy. Table 2 lists  $P$  and  $T_t$  from D11 that we use throughout our analysis<sup>4</sup>. We expand on the “Wilson Test” results by solving Kepler’s equations for the HRS RVs, while fixing  $P$  and  $T_t$  to their *a priori* values, yielding eccentricity,  $e$ , longitude of periastron,  $\omega$ , semi-major axes,  $K_A$  and  $K_B$ , and systemic velocity  $\gamma$ . We propagated the D11 uncertainty on  $P$  throughout the analysis, but simplified the procedure by using the D11 ephemeris  $T_t$  closest to our HRS observations and neglecting its uncertainty; the impact on the final  $q$ ,  $M_A$ , and  $M_B$  should be negligible. D11 derived precise values for  $e$ , and  $\omega$ , but because these are osculating parameters we chose to re-solve for them.

The TRES RVs reported by D11 constrain the spectroscopic orbit of Kepler-16A. We used the Levenberg-Marquardt fitting code MPFIT (Markwardt 2008) to solve Kepler’s equations for these RVs, yielding a purely spectroscopic set of parameters from the D11 results:  $e = 0.15983 \pm 0.00085$ ,  $\omega = 263.268^\circ \pm 0.040^\circ$ ,  $K_A = 13.666 \pm 0.012 \text{ km s}^{-1}$ ,  $\gamma_A = -32.7765 \pm 0.0061 \text{ km s}^{-1}$ , with reduced chi-squared of  $\chi_\nu^2 = 1.11$  and 15 degrees-of-freedom (DOF). An independent fit to our HRS primary

<sup>4</sup> The D11 Supporting Online Material incorrectly states that  $T_t$  is relative to BJD 2455000; actually, the values are given relative to BJD 2454900.

**Table 2**  
Kepler-16 Orbital Parameters and Stellar Masses

Parameter	Value
<i>Photometric-Dynamical Model (D11)</i>	
$P$ (days)	$41.077580 \pm 0.000008$
$T_t$	$2454965.657623 \pm 0.000058$
$e$	$0.15944^{+0.00061}_{-0.00062}$
$\omega$ (deg)	$263.464^{+0.026}_{-0.027}$
$i$ (deg)	$90.3401^{+0.0016}_{-0.0019}$
$a$ (AU)	$0.22431^{+0.00035}_{-0.00034}$
$q$	$0.2937 \pm 0.0006$
$M_A$ ( $M_\odot$ )	$0.6897^{+0.0035}_{-0.0034}$
$M_B$ ( $M_\odot$ )	$0.20255^{+0.00066}_{-0.00065}$
$R_A$ ( $R_\odot$ )	$0.6489^{+0.0013}_{-0.0013}$
$R_B$ ( $R_\odot$ )	$0.22623^{+0.00059}_{-0.00053}$
<i>SB2 Spectroscopy (this work)</i>	
$e$	$0.15894 \pm 0.00079$
$\omega$ (deg)	$263.287 \pm 0.041$
$K_A$ ( $\text{km s}^{-1}$ )	$13.642 \pm 0.010$
$K_B$ ( $\text{km s}^{-1}$ )	$45.56 \pm 0.47$
$\gamma_A$ ( $\text{km s}^{-1}$ )	$-33.7551 \pm 0.0064$
$\gamma_B$ ( $\text{km s}^{-1}$ )	$-33.32 \pm 0.35$
$q$	$0.2994 \pm 0.0031$
$M_A$ ( $M_\odot$ )	$0.654 \pm 0.017$
$M_B$ ( $M_\odot$ )	$0.1959 \pm 0.0031$

RVs gives  $e = 0.1602 \pm 0.0020$ ,  $\omega = 263.46^\circ \pm 0.12^\circ$ ,  $K_A = 13.598 \pm 0.022 \text{ km s}^{-1}$ , and  $\gamma_A = -33.770 \pm 0.018 \text{ km s}^{-1}$ , with  $\chi_\nu^2 = 1.58$  for 2 DOF. The HRS and TRES reference frames are offset by  $\sim 1 \text{ km s}^{-1}$ , which can be accounted for with an offset parameter; otherwise, the two solutions are in agreement, considering the paucity of HRS RVs.

We then simultaneously fit the HRS and TRES primary RVs and the HRS secondary RVs, accounting for the reference frame offset. The number of HRS secondary RVs is about four times fewer than the combined number of primary RVs, and they have much lower precision, so they do not further constrain  $e$  and  $\omega$ . Table 2 lists the resulting orbital parameters and mass ratio,  $q = 0.2994 \pm 0.0031$ , which is completely consistent with  $q$  derived from the “Wilson Test”, and Fig 3 shows the corresponding SB2 RV curves. This solution has  $\chi_\nu^2 = 1.013$ , with 25 DOF. Our velocity precision is sufficient to require different systemic velocities,  $\gamma_A$  and  $\gamma_B$ , for each star, due to the combined convective blue-shift and gravitational redshift of the two stars and templates (Pourbaix et al. 2002; Dravins 1999). We estimate the combined effect at  $\sim 400 \text{ m s}^{-1}$ , but did not attempt to disentangle the individual contributions. The uncertainty measured for  $\gamma_B$  implies that  $\gamma_A$  and  $\gamma_B$  differ by only  $\sim 1.25\sigma$ .

To examine the influence of systematic differences between the TRES and HRS RVs, we re-computed the orbital parameters using only the HRS data. As before,  $e$

and  $\omega$  are dominated by the primary RVs. This yields  $e$ ,  $\omega$ ,  $K_A$ , and  $\gamma_A$  that are numerically equivalent to the HRS SB1 derived above, and  $K_B$  and  $\gamma_B$  that are equivalent to the values in Table 2, with  $\chi^2_\nu = 1.12$  for 6 DOF. The resulting  $q = 0.2986 \pm 0.0032$  is identical to that derived from the ‘‘Wilson Test’’, and demonstrates that nearly all of the reported uncertainty is contributed by the secondary RVs: including or excluding the TRES RVs does not meaningfully change our derived masses or their precision.

Our measured  $K_A$  and  $K_B$  yield  $q = K_A/K_B = 0.2994 \pm 0.0031$  and, using the physical constants suggested by Harmanec & Prša (2011),  $M_A \sin^3 i = 0.654 \pm 0.017 M_\odot$  and  $M_B \sin^3 i = 0.1959 \pm 0.0031 M_\odot$ . When combined with the inclination measured by D11, we can solve directly for the dynamical masses of Kepler-16:  $M_A = 0.654 \pm 0.017 M_\odot$  and  $M_B = 0.1959 \pm 0.0031 M_\odot$ .

## 6. DISCUSSION

We have measured  $q$  to  $\sim 1\%$ , consistent with D11 at  $\sim 2\sigma$ , and  $M_B$  to  $\sim 1.5\%$ . We performed several tests to explore the  $q$  discrepancy and the robustness of our derived orbital parameters. Using the D11 orbit, we calculate predicted  $K_A = 13.661 \pm 0.030 \text{ km s}^{-1}$  and  $K_B = 46.512 \pm 0.076 \text{ km s}^{-1}$ . The difference between this  $K_A$  and our measured value reported in Table 2 cannot account for the  $q$  discrepancy. The difference between the predicted  $K_B$  and our measured value is  $2\sigma$ . An error in our measured  $K_B$  of  $\sim 1 \text{ km s}^{-1}$ , consistent with our reported uncertainty at  $2\sigma$ , would account for the discrepancy. However, the  $O_B - C_B$  residuals (Fig 3) suggest that our  $V_B$  uncertainties are overestimated.

Due to the small number of  $V_B$  measurements, a systematic error in one might skew our measured  $K_B$ . To test this, we repeated the KM fit six times, excluding each  $V_B$  in turn. This produced a range in  $K_B$  from  $45.36 \pm 0.59 \text{ km s}^{-1}$  to  $45.71 \pm 0.61 \text{ km s}^{-1}$ , corresponding to  $q$  from  $0.2984 \pm 0.0040$  to  $0.3007 \pm 0.0039$ , and  $\gamma_B$  from  $-33.21 \pm 0.40$  to  $-33.46 \pm 0.39$ . These distributions are symmetric around the values in Table 2, and confirm that no single HRS SB2 observation is skewing the measured  $q$ .

We considered that our analysis of the SB2 RVs might be affected by the planet’s orbital motion. However, this is unlikely because Kepler-16b has a nearly circular orbit with  $P \sim 229$  days (D11), while our HRS observations were obtained over just 28 days. None of our HRS observations coincided with a transit event, which would subject the RVs to a Rossiter-McLaughlin shift (Winn et al. 2011). Sunlight scattered off the moon might confuse our SB2 analysis, but the moon was down for three observations and at least  $70^\circ$  from Kepler-16 for the other three. No scattered light was detected in HRS sky fibers exposed coincident with our observations, so moonlight contamination is unlikely.

We have used dynamical SB2 measurements to derive  $q$ ,  $M_A$ , and  $M_B$  for the Kepler-16 EB, and have confirmed the  $q$  reported by D11 from their PDM to  $\sim 2\%$ . In addition, the  $e$  and  $\omega$  measured by the two techniques are equivalent. The claimed precision ( $q \sim 1\%$  by us and  $\sim 0.2\%$  by D11), results in a  $\sim 2\sigma$  disagreement that we cannot account for. It is possible that our measurement errors are underestimated due to an unidentified systematic effect, or that the D11 dynamical analysis is

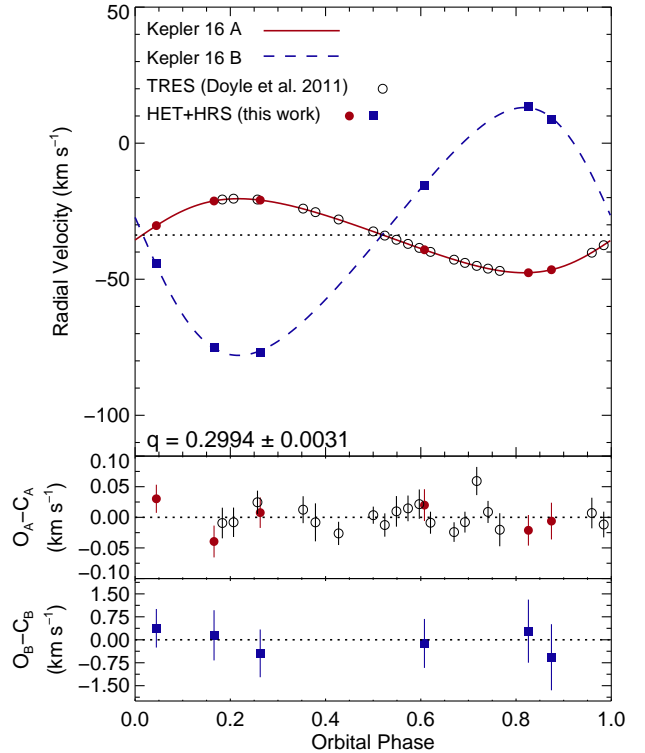


**Figure 3.** RV vs. orbital phase for Kepler-16A & B. *Upper Panel:* Solid circles and squares show our HRS  $V_A$  and  $V_B$ , respectively. Open circles show the D11 TRES  $V_A$ , offset to the HRS RV frame. The solid and dashed lines show the best orbital solution (Table 2). *Lower Panels:* Observed – calculated residuals for the HRS and D11 RVs.

erroneous, potentially due to the presence of additional bodies in the system. However, the latter is difficult to understand in light of the continued accuracy of transit and eclipse ephemerides in subsequent *Kepler* quarters of data (J. Carter, private communication). In addition to verifying the PDM result, we have demonstrated that masses with 1–2% precision can be measured for *Kepler* EBs, even when no planet transits are present.

We thank the referees, J. Carter, G. Torres, and L. Doyle, for a thorough report, and J. Carter for useful discussions about the D11 result prior to our initial submission of the manuscript. This work was partially supported by the Center for Exoplanets and Habitable Worlds, which is supported by the Pennsylvania State University, the Eberly College of Science, and the Pennsylvania Space Grant Consortium. We acknowledge support from the NAI, PSARC, and NSF grant AST-1006676. Data presented herein were obtained at the Hobby-Eberly Telescope (HET), a joint project of the University of Texas at Austin, the Pennsylvania State University, Stanford University, Ludwig-Maximilians-Universität München, and Georg-August-Universität Göttingen. The HET is named in honor of its principal benefactors, William P. Hobby and Robert E. Eberly.

## REFERENCES

- Allard, F., Homeier, D., & Freytag, B., 2011, ASPC, 448, 91
- Andersen, J., 1991, A&A Rev., 3, 91
- Bender, C. F., & Simon, M., 2008, ApJ, 689, 416
- Bender, C., Simon, M., Prato, L., Mazeh, T., & Zucker, S. 2005, AJ, 129, 402
- Borucki et al., 2010, Science, 327, 977
- Carter, J. A., Fabrycky, D. C., Ragozzine, D., et al. 2011, Science, 331, 562
- Chabrier, G., Gallardo, J., & Baraffe, I. 2007, A&A, 472, L17
- Clough, S. A., Shephard, M. W., Mlawer, E. J., Delamere, J. S., Iacono, M. J., Cady-Pereira, K., Boukabara, S., & Brown, P. D., 2005, J. Quant. Spec. Radiat. Transf., 91, 233
- Coughlin, J. L., López-Morales, M., Harrison, T. E., Ule, N., & Hoffman, D. L., 2011, AJ, 141, 78
- Cushing, M. C., Vacca, W. D., & Rayner, J. T. 2004, PASP, 116, 362
- Doyle, L. R., et al. 2011, Science, 333, 1602
- Dravins, D. 1999, IAU Colloq. 170: Precise Stellar Radial Velocities, 185, 268
- Eisenstein, D. J., et al. 2011, AJ, 142, 72
- Harmanec, P., & Prša, A. 2011, PASP, 123, 976
- Horner, J., Marshall, J. P., Wittenmyer, R. A., & Tinney, C. G. 2011, MNRAS, 416, 11
- Konacki, M. 2005, Nature, 436, 230
- Konacki, M. 2005, ApJ, 626, 431
- Konacki, M., Muterspaugh, M. W., Kulkarni, S. R., & Helminiak, K. G. 2010, ApJ, 719, 1293
- Leggett, S. K., Allard, F., Dahn, C., Hauschildt, P. H., Kerr, T. H., & Rayner, J. 2000, ApJ, 535, 965
- López-Morales, M. 2007, ApJ, 660, 732
- López-Morales, M., & Shaw, J. S. 2007, The Seventh Pacific Rim Conference on Stellar Astrophysics, 362, 26
- Markwardt, C. B. 2008, in ASP Conf. Ser. 411, Astronomical Data Analysis Software and Systems XVIII, ed. D. Bohlender, P. Dowler & D. Durand (San Francisco, CA: ASP), 251
- Murphy, M. T., Tzanavaris, P., Webb, J. K., & Lovis, C. 2007, MNRAS, 378, 221.
- Piskunov, N. E., & Valenti, J. A. 2002, A&A, 385, 1095
- Pourbaix, D., Nidever, D., McCarthy, C., et al. 2002, A&A, 386, 280
- Prša, A., et al. 2011, AJ, 141, 83
- Ramsey et al. 1998, Proc. SPIE, 3352, 34
- Ribas, I. 2006, Ap&SS, 304, 89
- Rowe et al. 2010, ApJ, 713, 150
- Shetrone et al. 2007, PASP, 119, 556
- Sigurdsson, S., Richer, H. B., Hansen, B. M., Stairs, I. H., & Thorsett, S. E. 2003, Science, 301, 193
- Slawson, R. W., et al. 2011, AJ, 142, 160
- Torres, G., Andersen, J., & Giménez, A. 2010, A&A Rev., 18, 67
- Tull, R. G., 1998, Proc. SPIE, 3355, 387
- Valenti, J. A., & Fisher, D. A. 2005, ApJS, 159, 141
- Welsh, W. F., et al. 2012, Nature, 10768
- Wilson, O. C. 1941, ApJ, 93, 29
- Wilson, J. C., et al. 2010, Proc. SPIE, 7735, 46
- Winn, J. N., et al. 2011, ApJ, 741, L1
- Wittenmyer, R. A., Horner, J., Marshall, J. P., Butters, O. W., & Tinney, C. G., 2012, 419, 3258
- York, D. G., et al. 2000, AJ, 120, 1579
- Zucker, S., & Mazeh, T. 1994, ApJ, 420, 806
- Zucker, S., Mazeh, T., Santos, N. C., Udry, S., & Mayor, M. 2003, A&A, 404, 775
- Zucker, S. 2003, MNRAS, 342, 1291